Radiation Physics and Chemistry xxx (xxxx) xxx–xxx

Contents lists available at ScienceDirect

Radiation Physics and Chemistry

journal homepage: www.elsevier.com/locate/radphyschem

Laboratory *operando* Fe and Mn K-edges XANES and Mössbauer studies of the $LiFe_{0.5}Mn_{0.5}PO_4$ cathode material

V.V. Shapovalov[a], A.A. Guda[a,*], N.V. Kosova[b], S.P. Kubrin[c], O.A. Podgornova[b], A.M. Aboraia[a,d], C. Lamberti[a,e], A.V. Soldatov[a]

[a] The Smart Materials Research Institute, Southern Federal University, Sladkova 178/24, 344090 Rostov-on-Don, Russia
[b] Institute of Solid State Chemistry and Mechanochemistry, Siberian Branch of the Russian Academy of Sciences, 18 Kutateladze, 630128 Novosibirsk, Russia
[c] Institute of Physics, Southern Federal University, Stachka Avenue 200/1, 344090 Rostov-on-Don, Russia
[d] Department of Physics, Faculty of Science, Al-Azhar University, Assiut 71542, Egypt
[e] Department of Physics, CrisDi and NIS Interdepartmental Centres and INSTM Reference Center, University of Turin, via Pietro Giuria 1, 10125 Turin, Italy

ARTICLE INFO

Keywords:
Li-ion batteries
Cathode materials
Operando XAS
Operando Mössbauer

ABSTRACT

We have developed and tested cell for laboratory operando diagnostics of Li-ion cathode materials. Local atomic and electronic structure of $LiFe_{1-x}Mn_xPO_4$ olivine cathode was studied by means of Fe and Mn K-edges XAS and Mössbauer spectroscopy. Analysis of XAS data allows us to follow the structural and oxidation state changes occurring during the cell cycling. Together with *operando* Mössbauer spectroscopy sensitive to the fine Fe ions local coordination distortions escaping from laboratory XANES, we are able to prove the homogeneity of Fe and Mn ions distribution.

1. Introduction

Li-ion batteries are widely used electrochemical energy storage devices (Andre et al., 2015). The olivine structured $LiFePO_4$ (LFP) cathode material is of particular interest to use in large-scale energy storage batteries for electrical vehicles, mobile devices and home power banks due to its structural, chemical and thermal stability (Chung et al., 2002). To increase the operating voltage of LFP, the Fe^{2+} ions are partially substituted by the Mn^{2+} ions, since the potential of the Mn^{2+}/Mn^{3+} redox couple (4.1 V) exceeds that of Fe^{2+}/Fe^{3+} (3.4 V). It has been found that the two-phase Li (de)intercalation mechanism, realized in micron-sized LFP, can be changed for a single-phase one in nanosized LFP. Meanwhile, the mechanism of the (de)lithiation processes in $LiFe_{1-x}Mn_xPO_4$ is still not fully understood.

For this purpose, the in situ and *operando* XRD and XAS studies of $LiFe_{1-x}Mn_xPO_4$ were performed in several synchrotron radiation centers (Drozhzhin et al., 2018; Le Toquin et al., 2006; Pelliccione et al., 2014; Sottmann et al., 2016; Piovano et al., 2011) XRD is used to probe long range order in the materials and to distinguish between single-phase or two-phase mechanism upon Li (de)intercalation (Kosova et al., 2012). Fe and Mn K-edges XANES probes the charge state of 3d metal ions and Jahn-Teller distortion of the nearest coordination spheres around absorbing atom (Nedoseykina et al., 2010).

Laboratory study is an important step before synchrotron characterization of the materials. The aim of the work was to develop the cell suitable for laboratory XAS and Mössbauer studies. It was successfully used to study *in operando* the charge-discharge processes in $LiFe_{0.5}Mn_{0.5}PO_4$ cathode material.

2. Methods

$LiFe_{0.5}Mn_{0.5}PO_4$ was prepared by the solvothermal synthesis by dissolving $FeSO_4{\cdot}7H_2O$, $MnCl_2{\cdot}2H_2O$, H_3PO_4, and LiOH in a molar ratio (Fe + Mn):P:Li = 1:1:3 as the starting materials, and ascorbic acid as a reducing agent to prevent oxidation of Fe^{2+} to Fe^{3+} in the solution of H_2O:EG = 1:1. The autoclave was heated to 200 °C and kept at this temperature for 3 h. Then, the sample was ball-milled with 3% of carbon and annealed at 750 °C for 1 h. The final product was phase pure with lattice parameters: $a = 10.3783$ Å, $b = 6.0433$ Å and $c = 4.7169$ Å.

Fe and Mn K-edge XANES spectra were collected in series in transmission mode with a Rigaku R-XAS spectrometer (Fig. 1b) equipped with 3 kW X-ray tube and Ge(311) monochromator. I_0 and I_1 were measured using an Ar-filled ionization chamber and a scintillation detector, respectively. Slits were used to size the X-ray beam on the sample position by 3 × 10 mm. The Mössbauer spectra were measured by MS1104Em Mössbauer spectrometer. The ^{57}Co in Rh matrix was used as a γ-ray source. The experimental spectra were fitted using SpectrRelax software (Matsnev and Rusakov, 2012). The isomer shifts

* Corresponding author.
E-mail address: guda@sfedu.ru (A.A. Guda).

https://doi.org/10.1016/j.radphyschem.2018.11.019
Received 30 September 2018; Received in revised form 12 November 2018; Accepted 19 November 2018

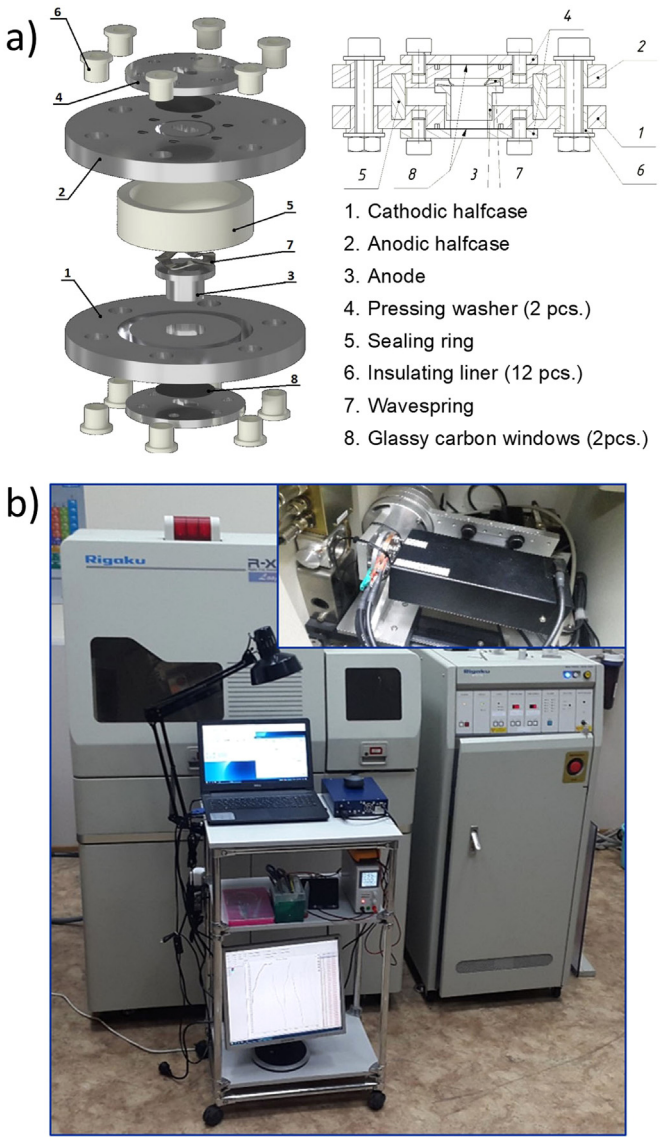

Fig. 1. (a): Assembly of the cell for laboratory XAS and Mössbauer studies. (b): Rigaku R-XAS spectrometer with the cell connected to galvanostat (see the inset).

were calculated with respect to the metallic α-Fe. The time required for the collection of a single spectrum was ca. 20 min for both Mössbauer and XANES (both edges) techniques.

For the electrochemical testing, the composite cathodes were fabricated by mixing 70 wt% of the active material with 25 wt% of carbon and 5 wt% of the PVDF/NMP binder. The working electrodes were dried at 40 °C for 12 h before cell assembly. The cell was assembled in an argon-filled glove box with Li as an anode, 1M $LiPF_6$ solution in a mixture of EC and DMC (1:1 by weight) as an electrolyte, and a glass fiber filter (Whatman, Grade GF/C) as a separator. Cycling was performed using a galvanostatic mode at C/25 charge/discharge rates within the voltage range of 2.0–4.5 V vs. Li/Li^+ at room temperature.

Operando experiments were carried out using in-house electrochemical cell (Fig. 1a). Conductivity and size of the cell windows become crucial for laboratory measurements due to difficulty in focusing the X-ray beam. Kapton foil is often used for these purposes though it can worsen electrochemical performance of the material due to poor electrical conductivity. Beryllium is the best candidate, but it is highly toxic when broken. Our cell was equipped with the X-ray transparent 300 μm thick glassy carbon windows. Design with the separate spring-loaded anode allows working with the electrode layers of variable thickness, which makes the cell suitable for the *operando* measurements with XANES, XRD and Mössbauer spectroscopy.

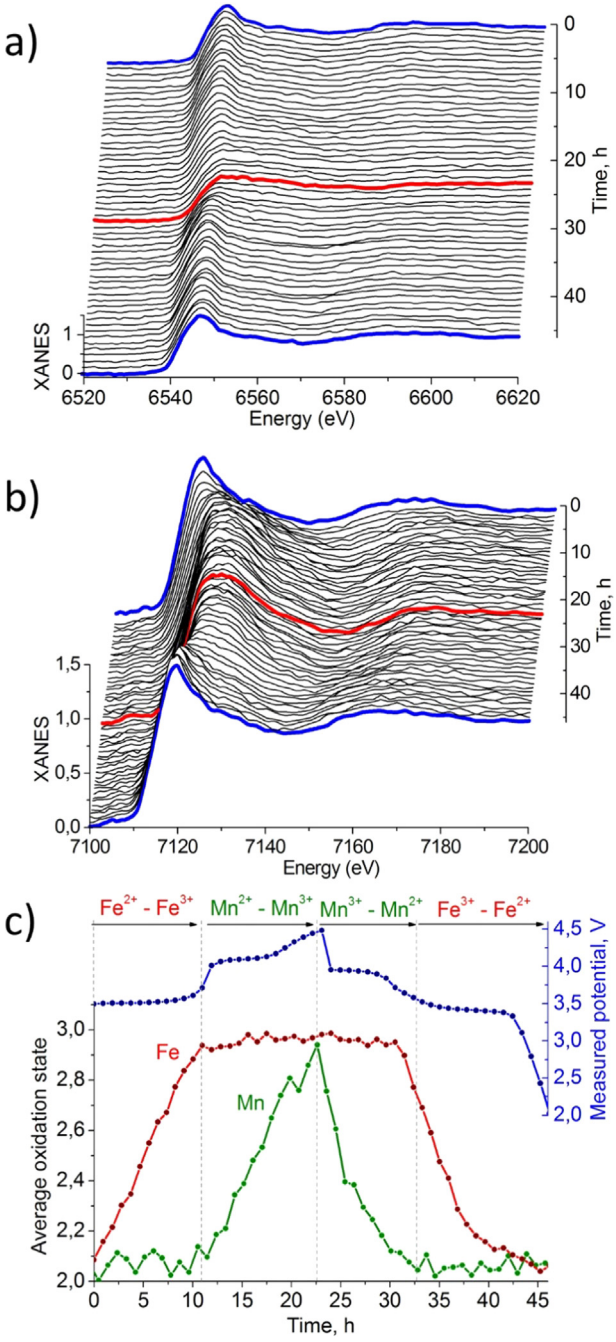

Fig. 2. (a): Mn K-edge XANES spectra measured during second charge and second discharge. (b): Fe K-edge XANES spectra measured during first charge and first discharge. (c): Mn and Fe charge states derived from the absorption edge position of the corresponding K-edge XANES spectra. The blue curve on top (right ordinate axis) reports the measured voltage.

3. Results and discussion

Fig. 2 shows XANES analysis of the Li intercalation/deintercalation processes in $LiFe_{0.5}Mn_{0.5}PO_4$. Panels (a) and (b) show the Fe and Mn K-edge spectra measured during the charge and discharge processes: blue curves correspond to the lowest potential (2 V) and red curve to the highest potential (4.5 V). Upon the charge, the absorption edge shifts

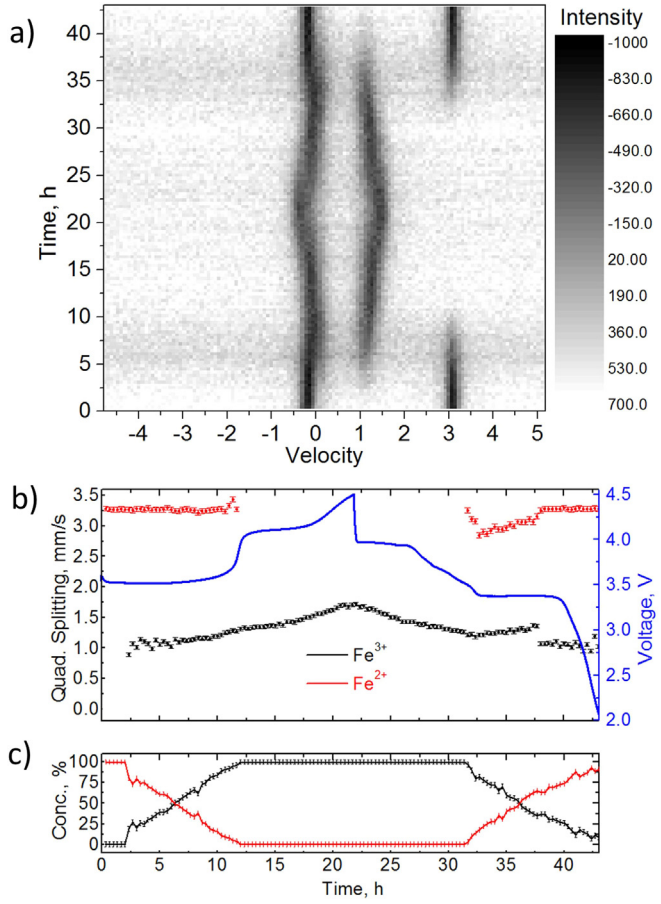

Fig. 3. (a): two-dimensional map constructed from the Mössbauer spectra measured continuously upon cell charge and discharge. (b): quadrupole splitting parameters obtained for two phases and the corresponding phase concentrations overlapped with the cell voltage profile, part (c).

towards higher energies pointing to the oxidation of metal. Fully reversible reduction is observed upon the discharge. Fig. 2c shows the charge state of Fe and Mn overlapped with the cell potential. The charge state was derived from the edge position compared to the reference compounds.

The analysis of the edge position for both Fe and Mn K-edges explains the features observed on the cell voltage profile (blue curve in Fig. 2c). The latter exhibits two separate plateaus. The first one located at 3.5 V corresponds to the Fe^{2+}/Fe^{3+} redox couple. The Mn oxidation state remains unchanged in this range. The second plateau at 4.1 V is responsible for the $Mn^{2+} \rightarrow Mn^{3+}$ redox transition. Within the experimental error, the Fe K-edge XANES remains unchanged at these voltages. This result is different from the data of the authors (Bezza et al., 2015) who observed a continuous variation in Fe edge position in $LiFe_{0.4}Mn_{0.6}PO_4$ olivine prepared by a sol-gel route.

Mössbauer spectra (Fig. 3a) reveal additional changes in the local atomic structure of iron. Fig. 3b shows the quadrupole splitting as a function of cell operational time. This parameter increases from 1 mm/s to 1.3 mm/s at the first plateau and from 1.3 mm/s to 1.6 mm/s at the second plateau. It is intriguing since, as learned from XANES, the Fe oxidation state remains unchanged at the second plateau. Larger values of the quadrupole splitting indicate the distortions of the oxygen octahedrons around the Fe atoms. If Mn and Fe atoms are distributed uniformly in the $LiFe_{0.5}Mn_{0.5}PO_4$ lattice, the $Mn^{2+} \rightarrow Mn^{3+}$ transition is accompanied by the strong Jahn-Teller effect which influences also the neighboring Fe atoms. These small variations escape from the laboratory XANES data but are clearly visible in the Mössbauer spectra as previously indicated by the other authors (Molenda et al., 2006).

It is known that delithiation of LFP occurs via the two-phase mechanism (LFPO and FPO), which was described by the shrinking core model or mosaic model for micron-sized material and by domino cascade model for nanosized material (Delmas et al., 2008). For $LiFe_{0.4}Mn_{0.6}PO_4$, the first-order phase transition was captured between three independent phases (Bezza et al., 2015). Recent advances in in situ characterization methods also provide direct experimental evidence of the solid-solution and intermediate-phase mechanisms during the $LiFePO_4$ phase transformation process under normal operating conditions (Wang and Sun, 2015). This was confirmed by findings of the extended solid solution and coherent transformations in $LiMn_{0.4}Fe_{0.6}PO_4$ via in situ synchrotron XRD, which explains the rate capability exceeding that of $LiFePO_4$ (Roberts et al., 2014). In our work, using the element and local sensitive XANES and Mössbauer spectroscopy, we address the microscopic structural changes in $LiMn_{0.5}Fe_{0.5}PO_4$ without discussion of the long-range order. From this point of view, the XANES data indicates the occurrence of the separate successive local transformations in the Fe and Mn coordination shells due to their oxidation during charge and reduction during discharge. Mössbauer spectroscopy indicates that Mn and Fe ions are uniformly distributed in the lattice and structural changes around Mn affect the iron coordination via increase in the quadrupole splitting. The fact that Fe and Mn redox processes are restricted by the corresponding plateaus on the voltage profile and are not overlapped implies the uniform Li distribution in the volume of the material upon cycling, and thus the occurrence of the first-order phase transitions in the whole structure. Additional information about phase transition mechanism can be obtained from the in situ XRD characterization of the material which is our further direction for development of cell for laboratory diagnostics.

4. Conclusions

We have developed and successfully tested the laboratory cell for *operando* XANES and Mössbauer studies of the cathode materials of Li-ion batteries. Equipped with large X-ray transparent conductive glassy carbon windows, the cell is applicable for nonfocused X-ray beams from laboratory equipment. The study was performed for the $LeFe_{0.5}Mn_{0.5}PO_4$ cathode material upon charge and discharge in the 2–4.5 V range at C/25 rate. In these conditions, the XANES spectra revealed the occurrence of the separated redox processes for Fe and Mn ions at the corresponding voltage plateaus (3.5 V and 4.1 V, respectively). Homogeneous distribution of Fe and Mn ions was further confirmed by monitoring the changes in the iron quadrupole splitting during the Mn^{2+}/Mn^{3+} oxidation. We demonstrated that laboratory measurements after appropriate analysis provide a reliable quantification of the d-metal charge state and local structural distortion.

Acknowledgements

VVS, AAG and AVS acknowledge the Russian Foundation for Basic Research (Project 17-02-01350/17) for the financial support.

References

Andre, D., Kim, S.-J., Lamp, P., Lux, S.F., Maglia, F., Paschos, O., Stiaszny, B., 2015. J. Mater. Chem. A 3, 6709–6732. https://doi.org/10.1039/C5TA00361J.

Bezza, I., Kaus, M., Heinzmann, R., Yavuz, M., Knapp, M., Mangold, S., Doyle, S., Grey, C.P., Ehrenberg, H., Indris, S., Saadoune, I., 2015. J. Phys. Chem. C 119, 9016–9024. https://doi.org/10.1021/jp513032r.

Chung, S.-Y., Bloking, J.T., Chiang, Y.-M., 2002. Nat. Mater. 1, 123. https://doi.org/10.1038/nmat732.

Delmas, C., Maccario, M., Croguennec, L., Le Cras, F., Weill, F., 2008. Nat. Mater. 7, 665. https://doi.org/10.1038/nmat2230.

Drozhzhin, O.A., Tereshchenko, I.V., Emerich, H., Antipov, E.V., Abakumov, A.M., Chernyshov, D., 2018. J. Synchrotron Radiat. 25, 468–472. https://doi.org/10.1107/S1600577517017489.

Kosova, N.V., Devyatkina, E.T., Ancharov, A.I., Markov, A.V., Karnaushenko, D.D., Makukha, V.K., 2012. Solid State Ion. 225, 564–569. https://doi.org/10.1016/j.ssi.2012.01.003.

Le Toquin, R., Paulus, W., Cousson, A., Prestipino, C., Lamberti, C., 2006. J. Am. Chem. Soc. 128, 13161–13174. https://doi.org/10.1021/ja063207m.
Matsnev, M.E., Rusakov, V.S., 2012. AIP Conf. Proc. 1489, 178–185. https://doi.org/10.1063/1.4759488.
Molenda, J., Ojczyk, W., Świerczek, K., Zając, W., Krok, F., Dygas, J., Liu, R.-S., 2006. Solid State Ion. 177, 2617–2624. https://doi.org/10.1016/j.ssi.2006.03.047.
Nedoseykina, T., Kim, M.G., Park, S.-A., Kim, H.-S., Kim, S.-B., Cho, J., Lee, Y., 2010. Electrochim. Acta 55, 8876–8882. https://doi.org/10.1016/j.electacta.2010.08.037.
Pelliccione, C.J., Timofeeva, E.V., Katsoudas, J.P., Segre, C.U., 2014. Rev. Sci. Instrum. 85, 126108. https://doi.org/10.1063/1.4904703.
Piovano, A., Agostini, G., Frenkel, A.I., Bertier, T., Prestipino, C., Ceretti, M., Paulus, W., Lamberti, C., 2011. J. Phys. Chem. C 115, 1311–1322. https://doi.org/10.1021/jp107173b.
Roberts, M.R., Madsen, A., Nicklin, C., Rawle, J., Palmer, M.G., Owen, J.R., Hector, A.L., 2014. J. Phys. Chem. C 118, 6548–6557. https://doi.org/10.1021/jp411152s.
Sottmann, J., Homs-Regojo, R., Wragg, D.S., Fjellvag, H., Margadonna, S., Emerich, H., 2016. J. Appl. Crystallogr. 49, 1972–1981. https://doi.org/10.1107/S160057671601428X.
Wang, J., Sun, X., 2015. Energy Environ. Sci. 8, 1110–1138. https://doi.org/10.1039/C4EE04016C.